HHS Public Access

Author manuscript

NanoImpact. Author manuscript; available in PMC 2018 January 01.

Published in final edited form as:

NanoImpact. 2017 January ; 5: 70–82. doi:10.1016/j.impact.2017.01.002.

Titanium Dioxide Nanoparticle Ingestion Alters Nutrient Absorption in an *In Vitro* Model of the Small Intestine

Zhongyuan Guo[1], **Nicole J. Martucci**[1], **Fabiola Moreno-Olivas**[1], **Elad Tako**[2], and **Gretchen J. Mahler**[1,*]

[1]Department of Biomedical Engineering, Binghamton University, Binghamton, NY, 13902

[2]Plant, Soil and Nutrition Laboratory, Agricultural Research Services, U.S. Department of Agriculture, Ithaca, NY

Abstract

Ingestion of titanium dioxide (TiO_2) nanoparticles from products such as agricultural chemicals, processed food, and nutritional supplements is nearly unavoidable. The gastrointestinal tract serves as a critical interface between the body and the external environment, and is the site of essential nutrient absorption. The goal of this study was to examine the effects of ingesting the 30 nm TiO_2 nanoparticles with an *in vitro* cell culture model of the small intestinal epithelium, and to determine how acute or chronic exposure to nano-TiO_2 influences intestinal barrier function, reactive oxygen species generation, proinflammatory signaling, nutrient absorption (iron, zinc, fatty acids), and brush border membrane enzyme function (intestinal alkaline phosphatase). A Caco-2/HT29-MTX cell culture model was exposed to physiologically relevant doses of TiO_2 nanoparticles for acute (four hours) or chronic (five days) time periods. Exposure to TiO_2 nanoparticles significantly decreased intestinal barrier function following chronic exposure. Reactive oxygen species (ROS) generation, proinflammatory signaling, and intestinal alkaline phosphatase activity all showed increases in response to nano-TiO_2. Iron, zinc, and fatty acid transport were significantly decreased following exposure to TiO_2 nanoparticles. This is because nanoparticle exposure induced a decrease in absorptive microvilli in the intestinal epithelial cells. Nutrient transporter protein gene expression was also altered, suggesting that cells are working to regulate the transport mechanisms disturbed by nanoparticle ingestion. Overall, these results show that intestinal epithelial cells are affected at a functional level by physiologically relevant exposure to nanoparticles commonly ingested from food.

Keywords

TiO_2; nanoparticles; ingestion; small intestine; nutrient absorption

*Correspondence to Gretchen Mahler, PhD, Binghamton University, Department of Biomedical Engineering, 2608 Biotechnology Building, Binghamton, NY 13902, Phone: 607-777-5238, Fax: 607-777-5780, gmahler@binghamton.edu.

1. Introduction

Engineered nanoparticles have become a commonly ingested material, and the effects of nanoparticles on gastrointestinal (GI) health and function are not well understood. Engineered nanoparticles (NP) exhibit specific physiochemical properties including unique optical effects, melting points, conductivity, ionization potential, electron affinity, magnetism, surface energy, reactivity, and potentially biological effects when compared to the bulk materials with the same mass dose[1–3]. The unique properties of NP stem from size, and the scale-dependent changes in the ratio of surface area to volume dramatically affect NP behavior. Volume decreases with size and the proportion of atoms at the particle surface increases, meaning that the number of atoms localized at the surface exponentially increases as the size decreases. This can increase the chemical reactivity and catalytic behavior per unit mass, and can alter absorption and excretion rates in biological systems such as DNA, proteins, and cell membranes[1–4]. Without a thorough understanding of the biological behavior of NP, it is impossible to predict the risks associated with NP exposure, and each new nanomaterial must be subject to health and safety assessment.

NP are increasingly used in food and food packaging applications, and companies are not required to seek regulatory approval before launching products containing nanosized ingredients made from approved bulk materials [5]. There are currently 150–600 nano foods and 400–500 nano food packaging applications containing nanotechnology-derived food ingredients, additives, supplements, and contact materials that are commercially available[6]. The dietary consumption of NPs in developed countries is estimated at more than 10^{12} particles/day, consisting mainly of titanium dioxide (TiO_2) and mixed silicates[6]. The European Food Safety Authority (EFSA), commissioning the Joint Research Centre (JRC), prepared an inventory of currently used and reasonably foreseen applications of nanomaterials in agriculture and food or feed production, and TiO_2 is the main type of engineered nanomaterial added to food[7]. TiO_2 NP exists in processed foods such as candies and chewing gums, and is primarily used as whitening agent due to its brightness, high refractive index, resistance to discoloration, and dispersion in water as a fairly stable colloid. Approximately 36% of food-grade TiO_2 (E171) are less than 100 nm in at least one dimension[8]. Personal care products, like toothpastes and some sunscreens, contain 1% to over 10% titanium by weight[8–10]. Human GI exposure to nanoparticles can occur in several ways. Nano-food ingredients, additives, and supplements from food packaging and contact materials that migrate into food can be ingested. Following consumption, nano-TiO_2 materials can enter the environment by treated effluent discharged to surface waters or biosolid application to agricultural land, for example, which can contribute to human exposure via drinking water or the food chain [2,8]. Due to the prevalence of nano-TiO_2 human ingestion is nearly unavoidable, which highlights the importance of studying the effects of TiO_2 NP ingestion.

In this study the two most common types of intestinal epithelial cells, absorptive and goblet, were represented by Caco-2 and HT29-MTX cells[11,12]. Caco-2 cells, which are derived from colonic epithelial adenocarcinoma cells, differentiate into a polarized, enterocyte-like epithelial barrier; express microvilli and tight junctions (TJ); and are capable of paracellular, transcellular, active, and transcytotic transport[13,14]. Caco-2 cells also express all of the major

amino acid, electrolyte, fatty acid, sugar/carbohydrate, iron, and zinc uptake, storage, transport, and carrier proteins[15–20]. The HT29-MTX cells are a subpopulation of HT29 human colonic adenocarcinoma cells selected for resistance to methotrexate (MTX), and mimic mucus secreting goblet-like cells[21]. When seeded at a ratio of 75% Caco-2 to 25% HT29-MTX and cultured for two weeks, a mucus layer that completely covers the cell monolayer and is 2–10 μm thick is formed[22]. This *in vitro* mucus layer is ~2/3 of the thickness of the duodenal firmly adherent mucus layer in humans (15 μm)[23].

Previous NP ingestion studies with this *in vitro* model[24] showed that following exposure to 10^9 50 nm carboxylated polystyrene nanoparticles/cm^2, iron transport, which is representative of iron transfer into the bloodstream, was significantly lowered. Exposure to the same size and concentration of NP also affected iron absorption in an *in vivo* chicken model. Ferritin analysis, divalent metal transporter 1 (DMT1) and nuclear factor kappa-light-chain-enhancer of activated B cells (NFκB1) gene expression, and histological examination demonstrated that the changes in iron absorption were not due to changes in transport protein expression or an inflammatory response, but instead, that exposure to NP significantly increased the overall villi volume. These experiments showed that data from the *in vitro* system correlates well with *in vivo* models, and that nanoparticle consumption alters intestinal function.

The overall goal of the current study is to determine if acute or chronic exposure to TiO_2 NP, which are commonly added to food and food packaging, affects small intestinal function. The interaction of 30 nm TiO_2 NP with Caco-2/HT29-MTX monolayers was evaluated by examining molecular, functional, and structural characteristics of the cells including nutrient transporter gene expression, reactive oxygen species (ROS) generation, Fe, Zn, or fatty acid absorption, alkaline phosphatase enzyme activity, TJ functionality, and microvilli structure. Transepithelial nutrient permeability is regulated by amino acid, electrolyte, fatty acid, sugar/carbohydrate, and mineral protein transporters, and is a highly regulated process[25]. Overall, these results show that exposure to physiologically relevant concentrations of TiO_2 NPs can have molecular, functional, and structural effects on intestinal epithelial cells.

2. Materials and Methods

30nm TiO_2 NP were purchased by US Research Nanomaterials, Inc. (Houston, TX). All culture flasks, plates, tubes, and pipette tips used for culturing cells were purchased from Corning (Corning, NY). All other chemicals, enzymes, and hormones were purchased from Sigma Aldrich (St. Louis, MO) unless otherwise stated. Glassware used in sample preparation and analysis was washed, soaked in 10% hydrochloric acid and 10% nitric acid overnight, and rinsed with 18 MΩ water to avoid iron or zinc contamination. All reagents were prepared in 18 MΩ water.

2.1. Nanoparticle Dose Calculations

In vitro doses of NP were formulated to represent potential real-life exposure. The total intestinal surface area is approximately 2×10^6 cm^2 [26] and the daily intake of nano-TiO_2 has been estimated to be 10^{12}–10^{14} NP per day, which is approximately 10^{11}–10^{13} particles per meal[27]. Ingesting 10^{13} NP exposes the small intestine to 10^6 particles/cm^2. If 10^{11} or 10^{13}

particles are ingested, the dose to the duodenum is approximately 10^8 or 10^{10} particles/cm^2, respectively. The duodenum is the first section of the small intestine, the site where most nutrient absorption occurs, and has approximately 900 cm^2 of absorbing surface area[28,29]. Supplemental Table 1 describes the low, medium, and high concentrations of 30 nm TiO_2 nanoparticles used for this study. When 100 μL of these solutions were added to 0.33 cm^2 cell monolayers, the concentrations were 10^6 particles/cm^2 (low), 10^8 particles/cm^2 (medium), and 10^{10} particles/cm^2 (high) for acute exposures. Chronic doses were three times (3X) the acute doses, representing the NP consumed in one day instead of one meal.

TiO_2 NP powder was weighed in a polystyrene weighing dish, and dispersed in sterile 18 MΩ water. Solutions were mixed uniformly in a sterile tube using a Thermolyne Mixer (Maxi Mix II, Type 37600) for 1 min, and then serially diluted to the concentrations shown in Supplemental Table 1. Nanoparticles solutions were placed in a sonicator (VWR® symphony™ Ultrasonic Cleaners, RF-48 W) for 30 min to break down NP agglomerates. The aqueous dispersions were then measured and used for *in vitro* model exposures.

2.2. Nanoparticle Characterizations

The distributions of TiO_2 NP sizes and average ζ-potentials were measured with a Zetasizer Nano ZS (Malvern Instruments Inc, Southborough, MA). Measurements were performed in Malvern disposable polycarbonate folded capillary cells with gold plated beryllium-copper electrodes (DTS1070), which were rinsed with ethanol, 18 MΩ water, and sample dispersions before readings. The Refractive Index (RI) value of TiO_2 is 2.42, and water RI is 1.33. Sample viscosities refer to the viscosity of water (0.8872 cP), and the dielectric constant of water is 78.5. The samples were equilibrated in the instrument chamber for 120 s, and measured at 25°C.

The TiO_2 NPs moved randomly in dispersants via Brownian Motion, and the size (hydrodynamic diameter, $d_{h,z\text{-average}}$) of the NP determined the speed of movement. The translational diffusion coefficient of particles and the intensity fluctuations in the scattered light were expressed in hydrodynamic diameter by Dynamic Light Scattering (DLS). Polydispersity index (PdI), generated by the Malvern software, is dimensionless and refers to the range of hydrodynamic diameter distribution. If PdI>0.5, NPs are polydisperse (polymodal) distributions [30]; PdI<0.1, represents monodisperse distributions [31].

A potential exists between the surfaces of the TiO_2 NPs and the dispersants, and the charge measurement is expressed in terms of ζ-potential.

The magnitude of the ζ-potential reflects the stability of the colloidal system. As the NPs in dispersants have a large negative or positive ζ-potential, they strongly repel each other to prevent particle aggregation. A solution is normally considered stable if the ζ-potential is more positive than +30mV or more negative than −30mV [32].

2.3. Transmission Electron Microscopy

The primary size and morphology of nano-TiO_2 dispersed in 18 MΩ water, DMEM and MEM were evaluated using transmission electron microscopy (TEM) on a JEOL JEM-2100F. Samples were diluted to 1.4×10^{-4} mg/ml from a stock dispersion of 14 mg/ml.

A drop of sample was loaded on an ultrathin 400 mesh copper TEM grid (Ted Pella, Inc) with a plastic transfer pipette. The grids were allowed to air-dry overnight before imaging.

2.4. Cell culture

The human colon carcinoma Caco-2 cell line was purchased from the American Type Culture Collection (Manassas, VA, USA) at Passage 17 and used in experiments at Passage 70–75. The HT29-MTX cell line was kindly provided by Dr. Thécla Lesuffleur of INSERM U560 in Lille, France, at Passage 11 and used in experiments at Passage 40–45. Both cell types were cultured in Dulbecco's Modified Eagle Medium (DMEM, Gibco® Thermo Fisher Scientific, Waltham, MA USA) with 10% (v/v) heat inactivated fetal bovine serum (HI-FBS, Gibco® Thermo Fisher Scientific, Waltham, MA USA). In experimental studies, Caco-2 and HT29-MTX were stained with trypan blue, counted with a hemocytometer, and resuspended at ratios of 75:25 (Caco-2/HT29-MTX), at a density of 100,000 cells/cm^2 onto polycarbonate, 0.4-μm pore size, 0.33 cm^2 membrane, 24-well Transwell® inserts (Corning Life Sciences) coated with rat tail Type I collagen (BD Biosciences, San Jose, CA, USA) at 8 μg/cm^2 for 1 hour at room temperature [33]. Cells were grown for 16 days to form a monolayer in a 37°C incubator with 5% CO_2, and culture medium was changed every 2 days. On the day before the *in vitro* exposure experiments, DMEM was removed and the monolayers were rinsed with Phosphate-buffered saline (PBS), and cultured overnight in very low iron and zinc minimal essential medium (MEM, Gibco®) supplemented with 10 mM PIPES, 4 mg/L hydrocortisone, 5 mg/L insulin, 5 μg/L selenium, 34 μg/L triiodothyronine, 1% antibiotic– antimycotic solution and 20 μg/L epidermal growth factor at pH 7.0 [34].

2.5. Transepithelial Electrical Resistance

Transepithelial electrical resistance (TER) of the monolayers was measured every three days after seeding in Transwell® inserts, and it was also measured before and after NP exposure with the EVOM2 and Endohm-6 chamber from World Precision Instruments (Sarasota, FL). The Endohm chamber was soaked in 70% ethanol for 15 min, 2 mL of sterile 100 mM KCl solution was added to the chamber, and the chamber was then connected to the EVOM2 which had a voltage reading between 0–20 mV. The old KCL solution was then removed and 600 μL fresh KCl was added into the Endohm chamber. A sterilized Calicell with 200μL KCL solution was inserted to the chamber and the Ohm reading was calibrated. After removing the Calicell, the Endohm chamber was rinsed with sterile 18 MΩ water three times, and then equilibrated with 2mL serum free DMEM for 15 minutes. After replacing the old medium with 600μL fresh serum free medium, the TER of every sample was measured three times at three different insert positions. The culture Transwells were taken out of incubator 5 minutes prior to measurements. Monolayer with TER values between 200 and 300 Ω×cm^2 were treated with nano-TiO_2 [35].

2.6. Acute and Chronic Exposure to NPs

Cells were rinsed once with PBS and then 600μL of MEM was placed into the basolateral chamber of the Transwells and 100μL culture medium containing low, medium, or high doses of TiO_2 NPs was placed into the apical chamber. In acute exposures the NP solutions were made in low mineral MEM. Cells were incubated at 37°C and 5% CO on a rocking

shaker (Laboratory Instrument Model RP-50, Rockville, MD) at 6 oscillations/minute for 4 hours. In chronic exposures the NP solutions were made fresh every day in DMEM+10% HI-FBS, and 100 μL was loaded into apical inserts. The basolateral medium and nano-TiO_2 solutions were changed daily for 5 days in chronic exposure treatments.

2.7. ^{58}Fe and ^{67}Zn uptake and transport

Mineral transport experiments were performed immediately after nanoparticle exposure. Stable isotope (^{58}Fe, ^{67}Zn) was added to the cells as 10 μM Fe(II)-ascorbate or 10 μM Zn(II)-ascorbate in serum free, very low mineral concentration MEM. The iron or zinc experimental medium was prepared immediately before use by combining ^{58}Fe or ^{67}Zn and 200 μL of 100 mM ascorbic acid (pH2). The molar ratio of Fe/Zn: ascorbic acid was 1:20. The mineral solutions sat at room temperature for 10 minutes, then 334 μL of 1.5 M NaCl was added, followed by 10 mL MEM. 100 μL of the mineral transport medium was added to the apical chamber immediately after nanoparticle exposure. Cells were incubated at 37°C and 5% CO_2 on a rocking shaker for 2 hours. The basolateral culture medium at bottom chamber was collected into a sterile 1.5 mL centrifuge tube, 10 μl HNO_3 was added, and the samples were stored at 4°C until ^{58}Fe and ^{67}Zn quantification with Inductively Coupled Plasma-Mass Spectroscopy (ICP-MS).

2.8. Inductively Coupled Plasma Mass Spectrometry Measurement

Stable isotope ratios in culture medium were determined via ICP-MS (ICAP Model 61E Trace Analyser; Thermo Jarrell Ash Corporation, Franklin, MA, USA). Samples were wet ashed with HNO_3 and $HClO_4$. Next 4 mL of 60/40 volume, double distilled 70% HNO_3/$HClO_4$ mixture and 0.25 mL of 40 mg/L Yttrium was added as an internal standard to each sample. Samples were incubated overnight at room temperature, then heated to 120°C in an aluminum heating block for 2 hours. If a sample did not clarify with this treatment, 0.25ml of concentrated nitric acid was added for further digestion until the temperature reached 195°C. Next, 20 mL of DI water was added, tubes were vortexed, and the solution was transferred into new glass tubes. Concentrations of ^{56}Fe and ^{58}Fe and ^{65}Zn and ^{67}Zn were determined. ^{72}Ge was added using a mixing-T just prior to the sample entering the nebulizer, serving as an internal standard. Hydrogen at 5 mL/min was used as a reaction gas to remove polyatomic interferences of Ar-O+ at mass 56. ^{58}Fe counts were corrected for ^{58}Ni using the natural abundance ratios of 2.59 (^{58}Ni/^{60}Ni). The concentrations of ^{67}Zn were determined similarly. The element concentrations were drift corrected and normalized using Yttrium as an internal standard. Data output from ICP-MS is expressed as mg/kg (ppm).

2.9 Fatty Acid Uptake

Caco-2/HT29-MTX cells cultured for 16 days in 96-well plates were immediately rinsed with 200μL cold medium after acute and chronic exposure. Cellular uptake studies of free fatty acids were performed using fluorescent BODIPY® 500/510 C1, C12 (4, 4-Difluoro-5-Methyl-4-Bora-3a, 4a-Diaza-s-Indacene-3-Dodecanoic Acid, ThermoFisher)[36–38]. Stock solutions were prepared in 5mmol/L ethanol solution, and stored at −20°C. The analogs were added to the culture medium to obtain a final concentration of 50 μmol/L in DMEM, 50μL to each well, and labeling was performed for 10 min. After 10 min the medium was quickly replaced by analog-free medium, and the cells cultured for an additional 1 h at 37°C

and 5% CO_2. Fluoresce in each well was measured using a with a fluorescent plate reader (Biotek Synergy 2, Winooski, VT, excitation/emission, 490/530).

2.10. Alkaline Phosphatase Activity Assay

TiO_2 exposure also significantly altered brush border membrane enzyme functionality. Monolayers were seeded into 24 well plates and exposed to medium or high concentrations of 30 nm TiO_2 for acute (4 hours) or chronic (5 days) time periods. Following exposure, cells were washed with 0.5 mL of PBS and then sonicated for 5 minutes at room temperature in 0.2 mL PBS. To recover the cell lysate each well was scraped into individual 1.5 mL centrifuge tubes.

The alkaline phosphatase (AP) assay detects the presence of alkaline phosphatase activity by using p-nitrophenyl phosphate (pNPP) as the substrate. The pNPP solution was made by dissolving one Tris Buffer tablet and one pNPP tablet (Sigma Aldrich, St. Louis MO) in 5mL of 18 MΩ water. AP hydrolyzes pNPP to p-nitrophenol, which turns bright yellow based on the concentration present. 25 μL of cell lysate solution from each tube was added to each well of a 96-well plate. 85 μL of the pNPP solution was then added to the wells. The plate was then incubated at room temperature for 1 hour. The absorbance was read on a plate reader at 405 nm to measure to concentration of p-nitrophenol.

The Bradford assay was used to determine the total cell protein concentration. 5 μL of cell lysate was added to a 96 well plate. 250 μL of Bradford Reagent was then added to each well. After incubating for 15 minutes at room temperature, absorbance was read at 595 nm using a plate reader. For each assay, a standard curve was created with p-nitrophenol (for the AP assay) or bovine serum albumin (BSA, for the Bradford assay) to calculate the unknown concentrations of p-nitrophenol or protein.

2.11. Scanning Electron Microscopy

Caco-2/HT29-MTX cells were seeded into 6-well plates containing sterilized cover slips coated with 8 $\mu g/cm^2$ rat tail Type I collagen and cultured for 16 days. The monolayers were acutely (4 hours) or chronically (5 days) exposed to TiO_2 NP in DMEM. The samples were then fixed in 4% paraformaldehyde, then rinsed by phosphate-buffered saline (PBS), dehydrated using an ethanol gradient (50, 75, 95,100 and 100%), transferred to hexamethyl disilizane (HMDS) and dried overnight (1:2 HMDS: Ethanol, 2:1 HMDS: Ethanol, 100% HMDS). Samples were then mounted, carbon coated, and viewed using a Zeiss Supra 55 Scanning Electron Microscope (Oberkochen, Germany) at 5k eV.

2.12. Gene Expression

Following NPs exposure and mineral transport studies, cells were processed for gene expression analysis. Total RNA was extracted using a Qiagen RNeasy Mini Kit. After exposure to NP, cells on Transwell inserts were released from the membrane with a cell scraper and provided lysis buffer. The cell lysate was homogenized with a QIAshredder column (Qiagen) and the RNA was isolated according to the manufacturer's instructions. Purified RNA was eluted in water and stored at −80°C. RNA was reverse transcribed to cDNA using the SuperScript III RT-PCR kit with oligo(dT) primer (Invitrogen). Primer

sequences are shown in Supplemental Table 2. The genes encoding DcytB, DMT1, HEPH, FPN1, FABP, FABP2, ZnT1, ZIP1, SGLT-1, IL-8, TNF-α, and NFκB were analyzed. Real-time polymerase chain reaction (RT-PCR) was performed in a MiniOpticon Real-Time PCR Detection System (Biorad). The 20 μL PCR mixtures consisted of 10 μL of POWER SYBR Green PCR Master Mix (Applied Biosystems, Carlsbad, CA), 7 μL of water, and 1 μL of each primer that was added to 1 μL of the cDNA samples. All reactions were performed in duplicates and under the following conditions: 95°C for 3 min, 50 cycles of 95°C for 60 s, 54°C for 15s, and 72°C for 30s. After the cycling process was completed, melting curves was determined from 65.0°C to 95.0°C with increment 0.5°C for 5s in order to ensure amplification of a single product. Expressions of the different genes were normalized to the expression of GADPH and compared with unexposed controls.

2.13. Reactive Oxygen Species Generation

Following NP exposure and mineral transport, 5 μmol/L of CellROX® Reagent (Thermo Fisher Scientific, excitation/emission 485/520) in MEM solution was added to the cells and incubated for 30 minutes at 37°C. Then medium was then removed, cells were rinsed three times with PBS, and ROS generation was measured with a fluorescent plate reader.

2.14. Immunocytochemistry

Cells exposed to CellROX® Reagent were fixed in 4% paraformaldehyde (PFA). 100 μL PFA was added to top well of plate for 1 hour. After fixing, cell monolayers were rinsed with PBS and 100 μL 0.1% solution of Triton X-100 in PBS was added to the top well, 600 μL to the bottom well for 5 minutes to permeabilize the cells. After the 5 minutes, an aliquot of 100 μL 5% Bovine Serum Albumin (BSA) in PBS solution was added to the top well and 600 μL to bottom well, and plates were rotated for 1 hour on a rocking platform. Cells were next incubated for 2 hours with 25 μL of 1:100 dilution of mouse anti-occludin primary antibody (Thermo Fisher Scientific), and then 2 hours with 25 μL 1:100 dilution of Alexa Fluor 568 goat anti-mouse secondary antibody (Thermo Fisher Scientific). The experiment was performed at room temperature, and cells were rinsed with PBS between each step. DNA was stained with 25 μL1:1000 solution of DRAQ5 (Thermo Fisher Scientific) in PBS for 30 minutes in the dark. After rinsing the cells with 18MΩ water, the membranes were removed and mounted on glass slide with ProLong Gold mounting medium (Thermo Fisher Scientific), and allowed to sit overnight in the dark. Finally, slides were sealed before imagining with a Leica TCS SP5 confocal microscope.

2.15. Statistics

All measurements were made at least 3 times for 2 separate experiments (n = 6) for each treatment. Results are expressed as mean ± standard error. Data was analyzed with the GraphPad Prism version 4.00 for Windows (GraphPad Software, San Diego, CA). A one-way ANOVA with Tukey's posttest or an unpaired Student's t-test was used to compare differences between means, and data was transformed when necessary to obtain equal sample variances. Differences between means were considered significant at $p < 0.05$.

3. Results

3.1 Nanoparticle Characterization

High-resolution TEM analysis (Figure 1A) demonstrated that the sizes of primary TiO_2 NP ranged from 20 to 40 nm, which were similar to the sizes given by the manufacturer. As shown in Supplemental Table 1, DLS measurement of hydrodynamic sizes ($d_{h,z\text{-average}}$) of TiO_2 NP were in the range of 300–2000 nm in dispersants. The much larger hydrodynamic diameter suggests that TiO_2 NP were aggregated, which is shown in the lower magnification TEM images that displayed the coexistence of larger TiO_2 agglomerates (Figure 1B). The $d_{h,z\text{-average}}$ of TiO_2 NPs in MEM were larger than in 18 MΩ water and DMEM. PdI values (Supplemental Table 1) in 18 MΩ water (0.34–0.49) and DMEM (0.42–0.54) were smaller than in MEM, which varied between 0.54 and 0.71. TiO_2 NPs in 18 MΩ water and DMEM therefore have relatively monodisperse size distributions and greater NP aggregation contributed to higher PdI values in MEM dispersant. Using lower concentration (1×10^{-3} mg/ml) of NP dispersions for DLS measurements helped to improve measurement accuracy [39].

Environmental pH and ions may also alter the surface charge density of nano-TiO_2 [32,40]. The pH values decreased from ~6.5 in 18 MΩ Water to 3.5 in 18 MΩ Water-^{58}Fe(II)/^{67}Zn(II)-ascorbate. The NP ζ-potential changed from −18mV in 18 MΩ water to 5mV in 18 MΩ water-^{58}Fe(II)/^{67}Zn(II)-ascorbate with the consequence of NP aggregation, as the electrostatic repulsion, which prevents aggregation, was inferior to the van der Waals forces that universally attract particles together [41]. The ζ-potentials of TiO_2 NP in MEM-^{58}Fe(II)/^{67}Zn(II)-ascorbate were in the range from −10mV to −13mV, which was statistically the same as ζ-potentials in MEM without Fe and Zn. This means that the TiO_2 NP did not bind a significant amount of Fe or Zn to the surface.

3.2 Tight Junction Functionality

TJs are continuous, belt-like and apical-most adhesive junctional complexes around mammalian epithelial cells [25]. Staining for the TJ protein occludin and measuring the transepithelial resistance (TER) are two common methods for evaluating epithelial monolayer integrity and TJ functionality. The Caco-2 and HT29-MTX monolayer confluence was quantitatively measured with TER, the magnitude of which represented the intactness of the monolayer. If nano-TiO_2 disrupted the monolayer integrity by either killing cells or breaking TJs, the TER values would decrease proportionally to the amount of damage to the epithelial layer. In acute exposures the nano-TiO_2 solution was applied once at the beginning of the experiment, and following NP exposure the TER values did not have any significant differences from unexposed controls (Figure 2A). The acute doses of TiO_2 NPs also had no effect on occludin expression (Supplemental Figure 1). In contrast, in monolayers exposed chronically to NP, after a 2-day exposure to low, medium, and high doses of nano-TiO_2 particles the TER dropped significantly below the control value (Figure 2B). A decrease in TER indicates that the doses of TiO_2 NPs were increasing the permeability of the TJs and allowing more passive diffusion between cells. An increased permeability is a sublethal toxic outcome, but interrupted barrier function of the intestinal epithelium can allow materials to diffused freely into the blood circulation from the

intestinal lumen [42]. The TER values of chronically exposed monolayers decreased to ~160Ω×cm^2 following a medium dose 5 day chronic exposure, but remained above 200Ω×cm^2 under high and low exposures and therefore did not cause epithelial cells to completely lose barrier function.

Staining for occludin proteins showed continuous ring appearance between adjacent cells before incubation with NPs (Supplemental Figure 1). After acute and chronic exposure, the staining for occludin proteins did not appeared discontinuous, which indicated that there were no openings of cell TJs in the monolayer. Comparatively, chronic TiO_2 NP exposure enlarged the gaps between cells or interrupted the TJ integrity (Supplemental Figure 1D, F).

3.3. Reactive Oxygen Species Formation

TiO_2 NP exposure resulted in the formation of oxidative stress in intestinal epithelial cells. The mean fluorescent signal intensities of ROS indicator significantly increased, indicating ROS is produced in response to acute or chronic TiO_2 exposure (Figure 2C–F). ROS can damage macromolecules, including DNA, oxidize polyunsaturated fatty acids in lipids and amino acids in proteins, break the structures of specific enzymes[43], and can also play an important role during the induction of apoptotic cell death [44,45].

3.4. Mineral Transport and Uptake

Mineral uptake, which is the amount of nutrient taken up into the cells, and mineral transport, which is representative of nutrient absorption into the bloodstream, are sensitive to NP exposure at realistic food doses. Following acute exposure, TiO_2 NP significantly decreased iron transport at medium and high doses, significantly decreased zinc transport at a medium dose, and significantly decreased iron uptake at a low dose (Figure 3A,C,E,G). Following chronic exposure, TiO_2 NP significantly decreased iron transport at medium and high doses, significantly decreased zinc transport at a medium dose, nutrient transport, Acute NP exposure significantly decreased Fe transport at medium and high doses, and chronic medium doses significantly decreased Fe transport (Figure 3A, C). Zn transport was significantly decreased following an acute exposure to a medium TiO_2 NP dose (Figure 3B, D). Nutrient uptake was not strongly affected by NP exposure (Figure 3E,F,G,H). Low, acute doses of TiO_2 NP significantly decreased iron uptake into the Caco-2/HT29-MTX monolayers and medium, chronic doses of TiO_2 NP significantly decreased zinc uptake. High chronic doses of TiO_2 NP significantly increased zinc uptake into the monolayers.

3.5. Intestinal Fatty Acid Uptake

Dietary fat supplies 30–40% of the average Western adult's daily caloric intake. Fat (primarily long-chain triglycerides) is hydrolyzed by pancreatic lipases to monoglycerides and free fatty acids that are emulsified with bile acids to form mixed micelles[46]. Fatty acids are absorbed by intestinal enterocytes by both passive diffusion and protein-facilitated transfer. One protein that may play an important role in fatty acid absorption is fatty acid–binding protein (FABP), which is expressed more heavily in the intestinal villi when compared with crypts[47]. Fluorescent fatty acid analogs were taken up by Caco-2/HT29-MTX monolayers from the apical Transwell chamber. Acute exposure to TiO_2 did not

significantly alter fatty acid uptake by cells, but a high, chronic dose of TiO_2 NP significantly decreased fatty acid uptake (Figure 3I, J).

3.6. Alkaline Phosphatase

TiO_2 NP exposure also significantly altered brush border membrane enzyme functionality. Figure 3K shows that acute medium and high TiO_2 NP exposure significantly increased intestinal alkaline phosphatase (IAP) activity. Figure 3L shows that chronic exposure to medium and high doses of TiO_2 also significantly increases IAP activity, and that IAP activity for chronically exposed cells is ~70% higher than acutely exposed cells.

3.7. Gene expression

Nano-TiO_2 exposure significantly decreased gene expression of the Fe transport proteins Dcytb, DMT1, HEPH, and FPN1, which were downregulated 0.44±0.03, 0.12±0.02, 0.21±0.04, and 0.62±0.05 fold, respectively, in response to chronic doses with ^{58}Fe (Figure 4C). DMT1 gene expression significantly decreased (0.31±0.08 fold) and Dcytb gene expression significantly increased (3.18±0.55 fold) following TiO_2 NP exposure with ^{65}Zn (Figure 4D). TiO_2 NPs significantly downregulated gene expressions of ZIP1 to 0.44±0.06 fold in response to chronic exposure to all three doses with ^{58}Fe (Figure 4C). Gene expression of ZnT1 was decreased to 0.33±0.03 fold following a medium, chronic dose of with ^{58}Fe (Figure 4C). Nano-TiO_2 particles significantly increased gene expressions of FABP1 and FABP2 to 2.11±0.29 and 2.62±0.39 fold respectively in response to a medium, chronic dose of TiO_2 NP with ^{58}Fe (Figure 4C). FABP2 gene expression was significantly upregulated 2.09±0.52 fold following chronic exposure to a low dose with ^{65}Zn (Figure 4D). Nutrient and fatty acid transport pathways and TJ protein components are summarized in Figure 5.

Proinflammatory gene expression was also analyzed. TiO_2 NPs upregulated expression of IL-8 following chronic NP exposure (3.59±0.56 fold, Figure 4 C and D). Nano-TiO_2 significantly increased TNFα and NFκB1 gene expression (5.20±1.15, 2.56±0.47 fold increase, respectively) was upregulated following chronic exposure (Figure 4 C, D).

3.8 Microvilli Structure

Figure 6 shows scanning electron microscopy images of Caco-2/HT29-MTX monolayer untreated controls (Figure 6A–D), following acute exposure to medium (Figure 6 E,F) or high (Figure 6 I, J) doses of TiO_2 NP, or following chronic exposure to medium (Figure 6 G,H) or high (Figure 6 K,L) doses of TiO_2 NP at varying magnification. Similar to results reported by Koeneman *et al.*[48], both acute and chronic nanoparticle exposure resulted in a decrease in absorptive cell microvilli.

4. Discussion

TiO_2 NP powder dispersed in water or medium resulted in NP agglomeration, even following sonication. The mean NP hydrodynamic diameter of the TiO_2 NPs was 300–500 nm (Supplementary Table 1) in water and medium, which is larger than endocytic vesicles (approximately 50–150 nm) and therefore likely partitioned the TiO_2 NP to the apical

surface of the monolayers[49]. Efforts to measure TiO_2 transport to the basolateral chamber with ICP-MS showed no TiO_2 transport across the Caco-2/HT29-MTX monolayers (data not shown). This agrees with work by Brun *et al.* who showed that, in vitro, TiO_2 nanoparticles are only transported by monolayers containing M cells[50]. A study by Jani *et al.* showed that 500 nm TiO_2 NP administered to female Sprague Dawley rats could translocate to the liver, spleen, lung and peritoneal tissues after oral gavage daily for 10 days[51], although the doses used were significantly higher (12.5 mg/kg) than those used in this study. Fisichella *et al.* found that doses of TiO_2 up to 100 μg/mL do not affect the viability of Caco-2 cells and determined that the particles are unlikely to enter the body via oral routes, although pristine NP did induce ROS production after a 72-hour exposure [52].

Because of the high surface free energy, TiO_2 NPs in biological medium absorb biological components, primarily proteins and amino acids [53]. In particular, proteins bind to the NPs surface and construct the protein corona or biological coating[54]. Doses of nano-TiO_2 particles in DMEM dispersant were coated by cell culture medium components (Figure 1C). Supplementary Table 1 shows that the average diameter of NP in DMEM+10% FBS is much smaller when compared with TiO_2 NP in serum free MEM. Previous work has shown that FBS at a typical concentration of 10% (v/v) improves TiO_2 NP dispersion, and that the NP "hard" protein corona can change based on the protein content of the solute[33,41,55]. Acute exposure studies were performed in serum-free, low mineral MEM, while the chronic exposure studies required DMEM+10% HI-FBS. The chronically exposed cells may therefore have been exposed to improved doses of NP with a "hard" corona, and this may have contributed to the greater effects seen due to chronic NP exposure.

TJs reside at the apical-most region of the paracellular space and polarize the intestinal epithelium into apical and basolateral regions by maintaining asymmetry in protein and lipid composition. As a selective/semipermeable paracellular barrier, dynamic, multiprotein TJ complexes restrict the ion, most solute, antigen, microorganism, and toxin transport through the intercellular space and prevent unwanted materials from entering systemic circulation [25]. The effects of TiO_2 NPs on the opening of TJs (measured by reduction in TER) was evaluated in the monolayers following acute and chronic exposure to three NP doses. TiO_2 NPs did not disrupt junctional complexes following acute exposures, as TER values were stable, and TER remained statistically the same between controls and TiO_2 NP-exposed cultures (Figure 2A). Chronic TiO_2 NP exposure significantly decreased TER to 150 $\Omega \times cm^2$, but most barrier function of the monolayers was maintained (Figure 2B). Occludin contributes to the barrier function of the TJs and possibly to the formation of aqueous pores within TJ strands[56]. Occludin staining showed that the morphology and lateral intercellular spaces in cell monolayers were not detectably changed following NP exposure, even at high doses and chronic exposures (Supplementary Figure 1).

Doses used in this study were relevant to real-life exposures from a single meal. These exposures were able to induce ROS generation (Figure 2C–H) and, following chronic dosing, significantly increased intestinal permeability (Figure 2B). Similar to ROS results in this study, De Angelis *et al.* found that TiO_2 NPs induced a high level of ROS formation in a dose-dependent manner in Caco-2 cells after 6 h, but did not induce IL-8 release or cytotoxicity [57]. Long-term (two months) exposure to low concentrations (1–50 μg/mL) of

TiO_2 NPs did not affect viability of A549 alveolar epithelial cells, but initiated oxidative damage to DNA and resulted in accumulated intracellular NPs [58]. The reduction in TER in this study was likely related to ROS formation, as cellular oxidative stress has been shown to activate redox-responsive signaling that disrupts TJ proteins[59]. Oxidative stress causes inflammation in gastrointestinal epithelial cells by producing proinflammatory cytokines such as IL-8 and TNF-α[60]. TNF-α is a major mediator of inflammation that activates NF-κB [61]. The proinflammatory mechanism induced by TNF-α can increase intestinal epithelial TJ permeability and contribute to intestinal inflammation as seen in Crohn's disease, for example[62]. The TER of filter-grown Caco-2 monolayers has been shown to display concentration-dependent decreases in permeability with TNF-α treatment[63]. The TNF-α-induced permeability correlated with NFκB activation, which in turn altered TJ protein localization and downregulated zonula occludens (ZO-1) proteins[63]. IL-8, TNF-α, and NFκB gene expression were upregulated following chronic TiO_2 NP exposure in the current study (Figure 4C, D), which shows the potential for even low doses of NP to induce inflammatory signaling with repeated exposure.

Almost all absorption and chemical digestion occur in the small intestine, which is divided into three unequal sections: the duodenum, the jejunum, and the ileum[64]. The duodenum is the first section of the small intestine and the site where most iron absorption occurs[67]. Intestinal iron absorption is regulated with body iron requirements and decreases when body iron stores increase[65,66]. Most dietary nonheme iron exists in form of ferric iron (Fe^{3+}) complexes in physiological conditions, whereas intestinal epithelium efficiently absorbs ferrous iron Fe^{2+} form, which is very unstable and quickly oxidized to ferric iron. Specialized transmembrane electron transport systems have evolved to reduce ferric Fe^{3+} form to ferrous iron Fe^{2+} form at the brush border extracellular surface [67]. Dcytb (duodenal cytochrome b) on the apical membrane plays an important role in ascorbate-dependent reduction of non-heme iron in the gut prior to uptake by the ferrous-iron transporter, DMT1[67–69]. Cellular iron is stored in the intracellular iron storage protein, ferritin, in order to both maintain large amounts of iron in a compact and bioavailable form in solution and protect the cell from oxidative damage [70]. Ferrous iron that reaches the basolateral membrane is oxidized back to ferric iron by the trans-membrane ferroxidase, hephaestin (HEPH), and then transported into the circulation by the iron export protein, ferroportin (FPN1), which co-localizes with HEPH in the basolateral membrane [65,67,68]. Dcytb, DMT1, HEPH, and FPN1 were downregulated in response to chronic medium and high doses of TiO_2 with ^{58}Fe (Figure 4C). The downregulation could be in response to the high iron content in the transport study medium or, for Dcytb and DMT1, because of the decrease in microvilli, which is where these proteins are expressed[71]. Iron transport was significantly affected by medium and high doses for both acute and chronic exposures (Figure 3A, B). Iron uptake, however, was only significantly reduced at low, acute doses of TiO_2 NP (Figure 3E). The alterations in nutrient transport were due to structural changes in the cell microvilli. TiO_2 exposure decreased the number of microvilli, which decreased the surface area available for nutrient transport (Figure 6). Koeneman *et al.*[48] has also reported that TiO_2 NPs (10 μg/mL) altered the microvillar organization on the apical surface of the epithelium following a 10-day treatment with TiO_2 NP[48]. Iron uptake was less affected because in the

Caco-2 model the iron transport phase is rate limiting[72], meaning that iron uptake occurs much faster than transport and is therefore less sensitive to cell alterations.

The jejunum has the highest rate of zinc absorption[73,74]. Zinc cannot cross biological membranes by simple diffusion because it is a highly-charged, hydrophilic ion and specialized mechanisms exist for its cellular uptake and release. Two families of mammalian zinc transporters regulate zinc levels in cytoplasm and intracellular. ZnT proteins, as members of the action diffusion facilitator family, move zinc across the lipid bilayer of the plasma membrane from the cytoplasm to the lumen of organelles or the extracellular space, and ZIP family is responsible for increasing intracellular zinc levels by either transporting the metal from the extracellular space or organelle lumen into the cytoplasm [75–79]. ZnT1 was the first zinc transporter cloned at the basolateral membrane of intestinal epithelial cells in the upper portion of the villus in the duodenum and jejunum. ZnT1 is regulated according to the amount of zinc in the diet, and mediates delivery of dietary zinc to the circulation [75,78–80]. The Zip1 protein is located in proximity to the apical microvilli in differentiated Caco-2 cells and it is responsible for intracellular Zn accumulation and transport[76]. As an intracellular sensor to regulate zinc homoeostasis, over expression of Zip1 results in upregulated uptake of Zn [76,81]. Zip1 and ZnT1 gene expression was significantly decreased only following chronic TiO_2 NP exposure in medium with Fe added (Figure 4C). This is consistent with studies by Yasuno et al. and Dufner-Beattie et al. that have shown that zinc transport is not correlated with zinc transporter mRNA expression in rats, and that ZIP gene expression is not regulated by dietary zinc[82,83]. Zinc transport across the cell monolayers was significantly decreased only by acute and chronic exposure to medium doses of TiO_2 NP (Figure 3C, D). Zinc uptake was significantly decreased by chronic medium doses of TiO_2 NP, and significantly increased by chronic high doses of TiO_2 NP (Figure 3H). The increase in zinc uptake at high TiO2 NP doses for chronic exposures was likely due to the increase in ROS formation (Figure 2F) and resulting inflammation. Proinflammatory conditions have been shown to increase Zn absorption[84,85], which allowed the cells to compensate for the loss of microvilli due to TiO_2 exposure

Cytoplasmic fatty acid binding proteins (FABPs) mediate fatty acid uptake and trafficking in small intestinal enterocytes. Two kinds of FABPs are largely present in the absorptive intestinal cells; liver-type FABP (LFABP; FABP1), and intestinal FABP (IFABP; FABP2)[86]. FABP1 and FABP2 were upregulated by medium dose chronic TiO_2 NP exposure with Fe (Figure 4C), and FABP2 was upregulated by low dose chronic TiO_2 NP exposure with Zn (Figure 4D). A high, chronic dose of TiO_2 NP resulted in a significant decrease in fatty acid (Figure 3J), likely because of the decreased surface area available for absorption due to damaged microvilli.

TiO_2 exposure also significantly altered brush border membrane enzyme functionality. Alkaline phosphatases are enzymes present in all tissues. In the small intestinal epithelium, IAP is responsible for the proper breakdown and adsorption of nutrients[87]. Recent work has shown that IAP regulates the absorption of lipids such as fatty acids across the apical intestinal epithelial membrane. Inhibition of IAP in mice on a high fat diet showed increased lipid transcytosis, visceral fat accumulation, and hepatic steatosis[88]. Many studies have shown evidence that IAP is a gut mucosal defense factor. For example, IAP can modulate

the pH of the intestinal epithelium surface in the duodenum, helping to prevent acid-induced duodenal injury by regulating bicarbonate secretion[89]. Following gut injury IAP is upregulated and prevents bacterial lipopolysaccharides from crossing the gut mucosal barrier[90]. In this study both medium and high doses of TiO_2 for acute and chronic exposures resulted in significantly increased IAP activity (Figure 4K, L).

5. Conclusions

TiO_2 exposure significantly affected Fe and Zn nutrient transport, fatty acid uptake, IAP activity, and tight junction functionality. Gene expression and ROS formation analysis showed NP exposure changed the expression levels of nutrient transport proteins and induced proinflammatory signaling. TiO_2 NP exposure decreased the number of intestinal microvilli, which decreased the surface area available for nutrient absorption. Overall, the results from this study indicate that intestinal epithelial cells are affected at a functional level by physiologically relevant exposure to TiO_2 NPs commonly ingested from food.

Supplementary Material

Refer to Web version on PubMed Central for supplementary material.

Acknowledgments

Funding: This work was supported by the Research Foundation of the State University of New York at Binghamton, the National Institutes of Health [grant number 1R15ES022828] and the CONACyT Fellowship.

References

1. Auffan M, Rose J, Bottero J-Y, Lowry GV, Jolivet J-P, Wiesner MR. Towards a definition of inorganic nanoparticles from an environmental, health and safety perspective. Nat Nano. 2009; 4:634–641.
2. Tiede K, Boxall ABA, Tear SP, Lewis J, David H, Hassellöv M. Detection and characterization of engineered nanoparticles in food and the environment. Food Additives & Contaminants: Part A. 2008; 25:795–821.
3. Jones CF, Grainger DW. In vitro assessments of nanomaterial toxicity. Advanced Drug Delivery Reviews. 2009; 61:438–456. [PubMed: 19383522]
4. Xia T, Li N, Nel AE. Potential Health Impact of Nanoparticles. Annual Review of Public Health. 2009; 30:137–150.
5. Powell JJ, Faria N, Thomas-McKay E, Pele LC. Origin and fate of dietary nanoparticles and microparticles in the gastrointestinal tract. Journal of Autoimmunity. 2010; 34:J226–J233. [PubMed: 20096538]
6. Martirosyan A, Schneider Y-J. Engineered nanomaterials in food: implications for food safety and consumer health. International journal of environmental research and public health. 2014; 11:5720–5750. [PubMed: 24879486]
7. Picó Y. Challenges in the determination of engineered nanomaterials in foods. TrAC Trends in Analytical Chemistry.
8. Weir A, Westerhoff P, Fabricius L, Hristovski K, von Goetz N. Titanium Dioxide Nanoparticles in Food and Personal Care Products. Environmental Science & Technology. 2012; 46:2242–2250. [PubMed: 22260395]
9. Chaudhry Q, Scotter M, Blackburn J, Ross B, Boxall A, Castle L, Aitken R, Watkins R. Applications and implications of nanotechnologies for the food sector. Food Additives & Contaminants: Part A. 2008; 25:241–258.

10. Gitrowski C, Al-Jubory AR, Handy RD. Uptake of different crystal structures of TiO2 nanoparticles by Caco-2 intestinal cells. Toxicology Letters. 2014; 226:264–276. [PubMed: 24576787]
11. Kararli TT. Comparison of the gastrointestinal anatomy, physiology, and biochemistry of humans and commonly used laboratory animals. Biopharmaceutics and Drug Disposition. 1995:16.
12. Forstner, JF., Forstner, GG. Gastrointestinal mucus. 3. Raven Press; 1994.
13. Artursson P, Karlsson J. Correlation Between Oral Drug Absorption In Humans And Apparent Drug Permeability Coefficients In Human Intestinal Epithelial Caco-2 Cells. Biochem Bioph Res Co. 1991; 175:880–885.
14. Artursson P, Palm K, Luthman K. Caco-2 monolayers in experimental and theoretical predictions of drug transport. Adv Drug Deliver Rev. 2001; 46:27–43.
15. Kipp H, Khoursandi S, Scharlau D, Kinne RKH. More than apical: distribution of SGLT1 in Caco-2 cells. American Journal of Physiology - Cell Physiology. 2003; 285:C737–C749. [PubMed: 12773314]
16. Halleux C, Schneider Y-J. Iron absorption by intestinal epithelial cells: 1. Caco-2 cells cultivated in serum-free medium, on polyethyleneterephthalate micropourous membranes, as an in vitro model. In Vitro Cell Developmental Biology. 1991; 27A:293–302.
17. Han OH, Wessling-Resnick M. Copper repletion enhances apical iron uptake and transepithelial iron transport by Caco-2 cells. American Journal of Physiology-Gastrointestinal and Liver Physiology. 2002; 282:G527–G533. [PubMed: 11842003]
18. Shen H, Qin H, Guo J. Cooperation of metallothionein and zinc transporters for regulating zinc homeostasis in human intestinal Caco-2 cells. Nutrition Research. 2008; 28:406–413. [PubMed: 19083439]
19. Levy E, Mehran M, Seidman E. Caco-2 cells as a model for intestinal lipoprotein synthesis and secretion. The FASEB Journal. 1995; 9:626–635. [PubMed: 7768354]
20. Hauri HP, Sterchi EE, Bienz D, Fransen JA, Marxer A. Expression and intracellular transport of microvillus membrane hydrolases in human intestinal epithelial cells. J Cell Biol. 1985; 101:838–851. [PubMed: 3897250]
21. Lesuffleur T, Barbat A, Dussaulx E, Zweibaum A. Growth Adaptation to Methotrexate of Ht-29 Human Colon-Carcinoma Cells Is Associated with Their Ability to Differentiate into Columnar Absorptive and Mucus-Secreting Cells. Cancer Res. 1990; 50:6334–6343. [PubMed: 2205381]
22. Mahler GJ, Shuler ML, Glahn RP. Characterization of Caco-2 and HT29-MTX cocultures in an in vitro digestion/cell culture model used to predict iron bioavailability. The Journal of Nutritional Biochemistry. 2009; 20:494. [PubMed: 18715773]
23. Atuma C, Strugala V, Allen A, Holm L. The adherent gastrointestinal mucus gel layer: thickness and physical state in vivo. American Journal Of Physiology-Gastrointestinal And Liver Physiology. 2001; 280:G922–G929. [PubMed: 11292601]
24. Mahler GJ, Esch MB, Tako E, Southard TL, Archer SD, Glahn RP, Shuler ML. Oral exposure to polystyrene nanoparticles affects iron absorption. Nat Nano. 2012; 7:264–270.
25. Groschwitz KR, Hogan SP. Intestinal barrier function: Molecular regulation and disease pathogenesis. Journal of Allergy and Clinical Immunology. 2009; 124:3–20. [PubMed: 19560575]
26. DeSesso JM, Jacobson CF. Anatomical and physiological parameters affecting gastrointestinal absorption in humans and rats. Food and Chemical Toxicology. 2001; 39:209–228. [PubMed: 11278053]
27. Lomer MCE, Thompson RPH, Powell JJ. Fine and ultrafine particles of the diet: Influence on the mucosal immune response and association with Crohn's disease. P Nutr Soc. 2002; 61:123–130.
28. Muir A, Hopfer U. Regional specificity of iron uptake by small intestinal brush-border membranes from normal and iron-deficient mice. Am J Physiol-Gastr L. 1985; 248:G376–G379.
29. Kararli TT. Comparison of the gastrointestinal anatomy, physiology, and biochemistry of humans and commonly used laboratory animals. Biopharm Drug Dispos. 1995:16.
30. Camli ST, Buyukserin F, Balci O, Budak GG. Size controlled synthesis of sub-100 nm monodisperse poly(methylmethacrylate) nanoparticles using surfactant-free emulsion polymerization. Journal of Colloid and Interface Science. 2010; 344:528–532. [PubMed: 20138293]

31. Bihari P, Vippola M, Schultes S, Praetner M, Khandoga AG, Reichel CA, Coester C, Tuomi T, Rehberg M, Krombach F. Optimized dispersion of nanoparticles for biological in vitro and in vivo studies. Particle and Fibre Toxicology. 2008; 5:1–14. [PubMed: 18269765]
32. Hanaor D, Michelazzi M, Leonelli C, Sorrell CC. The effects of carboxylic acids on the aqueous dispersion and electrophoretic deposition of ZrO2. Journal of the European Ceramic Society. 2012; 32:235–244.
33. Monopoli MP, Walczyk D, Campbell A, Elia G, Lynch I, Baldelli Bombelli F, Dawson KA. Physical-Chemical Aspects of Protein Corona: Relevance to in Vitro and in Vivo Biological Impacts of Nanoparticles. Journal of the American Chemical Society. 2011; 133:2525–2534. [PubMed: 21288025]
34. Glahn RP, Lee OA, Yeung A, Goldman MI, Miller DD. Caco-2 cell ferritin formation predicts nonradiolabeled food iron availability in an in vitro digestion/Caco-2 cell culture model. Journal of Nutrition. 1998; 128:1555–1561. [PubMed: 9732319]
35. Calatayud M, Vázquez M, Devesa V, Vélez D. In Vitro Study of Intestinal Transport of Inorganic and Methylated Arsenic Species by Caco-2/HT29-MTX Cocultures. Chemical Research in Toxicology. 2012; 25:2654–2662. [PubMed: 23116229]
36. Heller S, Cable C, Penrose H, Makboul R, Biswas D, Cabe M, Crawford SE, Savkovic SD. Intestinal inflammation requires FOXO3 and prostaglandin E2-dependent lipogenesis and elevated lipid droplets. American Journal of Physiology - Gastrointestinal and Liver Physiology. 2016; 310:G844–G854. [PubMed: 26968210]
37. Choe K, Jang JY, Park I, Kim Y, Ahn S, Park D-Y, Hong Y-K, Alitalo K, Koh GY, Kim P. Intravital imaging of intestinal lacteals unveils lipid drainage through contractility. The Journal of Clinical Investigation. 2015; 125:4042–4052. [PubMed: 26436648]
38. Stahl A, Hirsch DJ, Gimeno RE, Punreddy S, Ge P, Watson N, Patel S, Kotler M, Raimondi A, Tartaglia LA, Lodish HF. Identification of the Major Intestinal Fatty Acid Transport Protein. Molecular Cell. 1999; 4:299–308. [PubMed: 10518211]
39. Sikora A, Shard AG, Minelli C. Size and ζ-Potential Measurement of Silica Nanoparticles in Serum Using Tunable Resistive Pulse Sensing. Langmuir. 2016; 32:2216–2224. [PubMed: 26869024]
40. French RA, Jacobson AR, Kim B, Isley SL, Penn RL, Baveye PC. Influence of Ionic Strength, pH, and Cation Valence on Aggregation Kinetics of Titanium Dioxide Nanoparticles. Environmental Science & Technology. 2009; 43:1354–1359. [PubMed: 19350903]
41. Ji Z, Jin X, George S, Xia T, Meng H, Wang X, Suarez E, Zhang H, Hoek EMV, Godwin H, Nel AE, Zink JI. Dispersion and Stability Optimization of TiO2 Nanoparticles in Cell Culture Media. Environmental Science & Technology. 2010; 44:7309–7314. [PubMed: 20536146]
42. Ranaldi G, Marigliano I, Vespignani I, Perozzi G, Sambuy Y. The effect of chitosan and other polycations on tight junction permeability in the human intestinal Caco-2 cell line1. The Journal of Nutritional Biochemistry. 2002; 13:157–167. [PubMed: 11893480]
43. Martindale JL, Holbrook NJ. Cellular response to oxidative stress: Signaling for suicide and survival*. Journal of Cellular Physiology. 2002; 192:1–15. [PubMed: 12115731]
44. Chan W-H, Wu C-C, Yu J-S. Curcumin inhibits UV irradiation-induced oxidative stress and apoptotic biochemical changes in human epidermoid carcinoma A431 cells. Journal of Cellular Biochemistry. 2003; 90:327–338. [PubMed: 14505349]
45. Hengartner MO. The biochemistry of apoptosis. Nature. 2000; 407:770–776. [PubMed: 11048727]
46. Ros E. Intestinal absorption of triglyceride and cholesterol. Dietary and pharmacological inhibition to reduce cardiovascular risk. Atherosclerosis. 2000; 151:357–379. [PubMed: 10924713]
47. Wang TY, Liu M, Portincasa P, Wang DQH. New insights into the molecular mechanism of intestinal fatty acid absorption. European Journal of Clinical Investigation. 2013; 43:1203–1223. [PubMed: 24102389]
48. Koeneman BA, Zhang Y, Westerhoff P, Chen Y, Crittenden JC, Capco DG. Toxicity and cellular responses of intestinal cells exposed to titanium dioxide. Cell Biology and Toxicology. 2010; 26:225–238. [PubMed: 19618281]
49. Liang M, Lin IC, Whittaker MR, Minchin RF, Monteiro MJ, Toth I. Cellular uptake of densely packed polymer coatings on gold nanoparticles. ACS Nano. 2010:4.

50. Brun E, Barreau F, Veronesi G, Fayard B, Sorieul S, Chaneac C, Carapito C, Rabilloud T, Mabondzo A, Herlin-Boime N, Carriere M. Titanium dioxide nanoparticle impact and translocation through ex vivo, in vivo and in vitro gut epithelia. Part Fibre Toxicol. 2014; 11:13. [PubMed: 24666995]
51. Jani PU, McCarthy DE, Florence AT. Titanium dioxide (rutile) particle uptake from the rat GI tract and translocation to systemic organs after oral administration. International Journal of Pharmaceutics. 1994; 105:157–168.
52. Fisichella M, Berenguer F, Steinmetz G, Auffan M, Rose J, Prat O. Intestinal toxicity evaluation of TiO2 degraded surface-treated nanoparticles: a combined physico-chemical and toxicogenomics approach in caco-2 cells. Particle and Fibre Toxicology. 2012; 9:1–13. [PubMed: 22239852]
53. Mudunkotuwa IA, Grassian VH. Biological and environmental media control oxide nanoparticle surface composition: the roles of biological components (proteins and amino acids), inorganic oxyanions and humic acid. Environmental Science: Nano. 2015; 2:429–439.
54. Tenzer S, Docter D, Kuharev J, et al. Rapid formation of plasma protein corona critically affects nanoparticle pathophysiology. Nat Nano. 2013; 8:772–781.
55. Lynch I, Dawson KA. Protein-nanoparticle interactions. Nano Today. 2008; 3:40–47.
56. McCarthy KM, Skare IB, Stankewich MC, Furuse M, Tsukita S, Rogers RA, Lynch RD, Schneeberger EE. Occludin is a functional component of the tight junction. Journal of Cell Science. 1996; 109:2287–2298. [PubMed: 8886979]
57. De Angelis I, Barone F, Zijno A, Bizzarri L, Russo MT, Pozzi R, Franchini F, Giudetti G, Uboldi C, Ponti J, Rossi F, De Berardis B. Comparative study of ZnO and TiO2 nanoparticles: physicochemical characterisation and toxicological effects on human colon carcinoma cells. Nanotoxicology. 2013; 7:1361–1372. [PubMed: 23078188]
58. Armand L, Tarantini A, Beal D, Biola-Clier M, Bobyk L, Sorieul S, Pernet-Gallay K, Marie-Desvergne C, Lynch I, Herlin-Boime N, Carriere M. Long-term exposure of A549 cells to titanium dioxide nanoparticles induces DNA damage and sensitizes cells towards genotoxic agents. Nanotoxicology. 2016; 10:913–923. [PubMed: 26785166]
59. Chen L, Yokel RA, Hennig B, Toborek M. Manufactured Aluminum Oxide Nanoparticles Decrease Expression of Tight Junction Proteins in Brain Vasculature. Journal of Neuroimmune Pharmacology. 2008; 3:286–295. [PubMed: 18830698]
60. Katayama S, Xu X, Fan MZ, Mine Y. Antioxidative Stress Activity of Oligophosphopeptides Derived from Hen Egg Yolk Phosvitin in Caco-2 Cells. Journal of Agricultural and Food Chemistry. 2006; 54:773–778. [PubMed: 16448181]
61. Micheau O, Tschopp J. Induction of TNF Receptor I-Mediated Apoptosis via Two Sequential Signaling Complexes. Cell. 2003; 114:181–190. [PubMed: 12887920]
62. Ye D, Ma I, Ma TY. Molecular mechanism of tumor necrosis factor-α modulation of intestinal epithelial tight junction barrier. American Journal of Physiology - Gastrointestinal and Liver Physiology. 2006; 290:G496–G504. [PubMed: 16474009]
63. Ma TY, Iwamoto GK, Hoa NT, Akotia V, Pedram A, Boivin MA, Said HM. TNF-α-induced increase in intestinal epithelial tight junction permeability requires NF-κB activation. American Journal of Physiology - Gastrointestinal and Liver Physiology. 2004; 286:G367–G376. [PubMed: 14766535]
64. Martini, FH. Fundamentals of Anatomy and Physiology. 6. Prentice Hall, Inc; 2004.
65. Eady JJ, Wormstone YM, Heaton SJ, Hilhorst B, Elliott RM. Differential effects of basolateral and apical iron supply on iron transport in Caco-2 cells. Genes & Nutrition. 2015; 10:1–15.
66. Galy B, Ferring-Appel D, Becker C, Gretz N, Gröne H-J, Schümann K, Hentze Matthias W. Iron Regulatory Proteins Control a Mucosal Block to Intestinal Iron Absorption. Cell Reports. 2013; 3:844–857. [PubMed: 23523353]
67. McKie AT, Barrow D, Latunde-Dada GO, et al. An Iron-Regulated Ferric Reductase Associated with the Absorption of Dietary Iron. Science. 2001; 291:1755–1759. [PubMed: 11230685]
68. Lane DJ, Bae D-H, Merlot AM, Sahni S, Richardson DR. Duodenal cytochrome b (DCYTB) in iron metabolism: an update on function and regulation. Nutrients. 2015; 7:2274–2296. [PubMed: 25835049]

69. McCarthy RC, Kosman DJ. Iron transport across the blood–brain barrier: development, neurovascular regulation and cerebral amyloid angiopathy. Cellular and Molecular Life Sciences. 2015; 72:709–727. [PubMed: 25355056]

70. Arosio P, Levi S. Cytosolic and mitochondrial ferritins in the regulation of cellular iron homeostasis and oxidative damage. Biochimica et Biophysica Acta (BBA) - General Subjects. 2010; 1800:783–792. [PubMed: 20176086]

71. Gulec S, Anderson GJ, Collins JF. Mechanistic and regulatory aspects of intestinal iron absorption. American Journal of Physiology - Gastrointestinal and Liver Physiology. 2014; 307:G397–G409. [PubMed: 24994858]

72. Alvarez-Hernandez X, Nichols GM, Glass J. Caco-2 cell line: a system for studying intestinal iron transport across epithelial cell monolayers. Biochemica et Biophysica Acta. 1991; 1070:205–208.

73. Muir A, Hopfer U. Regional Specificity Of Iron Uptake By Small Intestinal Brush-Border Membranes From Normal And Iron-Deficient Mice. American Journal Of Physiology. 1985; 248:G376–G379. [PubMed: 3976894]

74. Lee HH, Prasad AS, Brewer GJ, Owyang C. Zinc absorption in human small intestine. American Journal of Physiology - Gastrointestinal and Liver Physiology. 1989; 256:G87–G91.

75. Lichten LA, Cousins RJ. Mammalian Zinc Transporters: Nutritional and Physiologic Regulation. Annual Review of Nutrition. 2009; 29:153–176.

76. Michalczyk AA, Ackland ML. hZip1 (hSLC39A1) regulates zinc homoeostasis in gut epithelial cells. Genes & Nutrition. 2013; 8:475–486. [PubMed: 23378263]

77. Desouki MM, Franklin RB, Costello LC, Fadare O. Persistent low expression of hZip1 in mucinous carcinomas of the ovary, colon, stomach and lung. Journal of Ovarian Research. 2015; 8:1–7. [PubMed: 25884701]

78. Lodemann U, Gefeller E-M, Aschenbach JR, Martens H, Einspanier R, Bondzio A. Dose Effects of Apical versus Basolateral Zinc Supplementation on Epithelial Resistance, Viability, and Metallothionein Expression in Two Intestinal Epithelial Cell Lines. Journal of Biochemical and Molecular Toxicology. 2015; 29:410–417.

79. Gefeller E-M, Bondzio A, Aschenbach JR, Martens H, Einspanier R, Scharfen F, Zentek J, Pieper R, Lodemann U. Regulation of intracellular Zn homeostasis in two intestinal epithelial cell models at various maturation time points. The Journal of Physiological Sciences. 2015; 65:317–328. [PubMed: 25757458]

80. McMahon RJ, Cousins RJ. Regulation of the zinc transporter ZnT-1 by dietary zinc. Proceedings of the National Academy of Sciences. 1998; 95:4841–4846.

81. Jou M-Y, Philipps AF, Kelleher SL, Lönnerdal B. Effects of zinc exposure on zinc transporter expression in human intestinal cells of varying maturity. Journal of pediatric gastroenterology and nutrition. 2010; 50:587–595. [PubMed: 20479680]

82. Yasuno T, Okamoto H, Nagai M, Kimura S, Yamamoto T, Nagano K, Furubayashi T, Yoshikawa Y, Yasui H, Katsumi H, Sakane T, Yamamoto A. In vitro study on the transport of zinc across intestinal epithelial cells using Caco-2 monolayers and isolated rat intestinal membranes. Biological & pharmaceutical bulletin. 2012; 35:588–593. [PubMed: 22466565]

83. Dufner-Beattie J, Langmade SJ, Wang F, Eide D, Andrews GK. Structure, Function, and Regulation of a Subfamily of Mouse Zinc Transporter Genes. J Biol Chem. 2003; 278:50142–50150. [PubMed: 14525987]

84. Pekarek RS, Evans GW. Effect of acute infection and endotoxemia on zinc absorption in the rat. Proceedings of the Society for Experimental Biology and Medicine. Society for Experimental Biology and Medicine. 1975; 150:755–758.

85. Sas B, Bremner I. Effect of acute stress on the absorption and distribution of zinc and on Zn-metallothionein production in the liver of the chick. Journal of inorganic biochemistry. 1979; 11:67–76. [PubMed: 383905]

86. Gajda AM, Storch J. Enterocyte Fatty Acid Binding Proteins (FABPs): Different Functions of Liver- and Intestinal- FABPs in the Intestine. Prostaglandins, leukotrienes, and essential fatty acids. 2015; 93:9–16.

87. Lallès J-P. Intestinal alkaline phosphatase: multiple biological roles in maintenance of intestinal homeostasis and modulation by diet. Nutrition Reviews. 2010; 68:323–332. [PubMed: 20536777]

88. Nakano T, Inoue I, Koyama I, et al. Disruption of the murine intestinal alkaline phosphatase gene Akp3 impairs lipid transcytosis and induces visceral fat accumulation and hepatic steatosis. American Journal of Physiology - Gastrointestinal and Liver Physiology. 2007; 292:G1439–G1449. [PubMed: 17332477]

89. Mizumori M, Ham M, Guth PH, Engel E, Kaunitz JD, Akiba Y. Intestinal alkaline phosphatase regulates protective surface microclimate pH in rat duodenum. The Journal of Physiology. 2009; 587:3651–3663. [PubMed: 19451200]

90. Goldberg RF, Austen WG, Zhang X, Munene G, Mostafa G, Biswas S, McCormack M, Eberlin KR, Nguyen JT, Tatlidede HS, Warren HS, Narisawa S, Millán JL, Hodin RA. Intestinal alkaline phosphatase is a gut mucosal defense factor maintained by enteral nutrition. Proceedings of the National Academy of Sciences. 2008; 105:3551–3556.

91. Furuse M, Hirase T, Itoh M, Nagafuchi A, Yonemura S, Tsukita S. Occludin: a novel integral membrane protein localizing at tight junctions. The Journal of cell biology. 1993; 123:1777–1788. [PubMed: 8276896]

92. Blikslager AT, Moeser AJ, Gookin JL, Jones SL, Odle J. Restoration of Barrier Function in Injured Intestinal Mucosa. Physiological Reviews. 2007; 87:545–564. [PubMed: 17429041]

93. Martínez C, González-Castro A, Vicario M, Santos J. Cellular and Molecular Basis of Intestinal Barrier Dysfunction in the Irritable Bowel Syndrome. Gut and Liver. 2012; 6:305–315. [PubMed: 22844557]

Highlights

- Ingestion of TiO_2 nanoparticles is nearly unavoidable.
- Intestinal epithelial cells were acutely and chronically exposed to 30 nm TiO_2.
- TiO_2 exposure affected nutrient absorption and enzyme activity.
- Nanoparticle exposure induced a significant decrease in absorptive microvilli.
- Intestinal cells are affected functionally by commonly ingested nanoparticles.

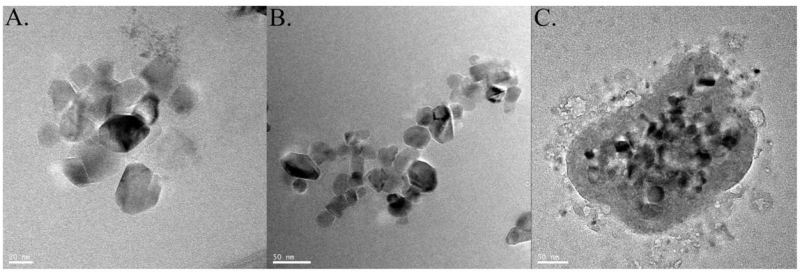

Figure 1.

Transmission electron microscopy. Titanium dioxide (TiO_2) nanoparticles in water dispersant at 1.2×10^{-3} mg/ml, 20nm scale bar (A); nano-TiO_2 in water dispersant at 2.5×10^{-2} mg/ml, 50nm scale bar (B); and TiO_2 nanoparticles in DMEM dispersant at 1.2×10^{-3} mg/ml, 50 nm scale bar (C).

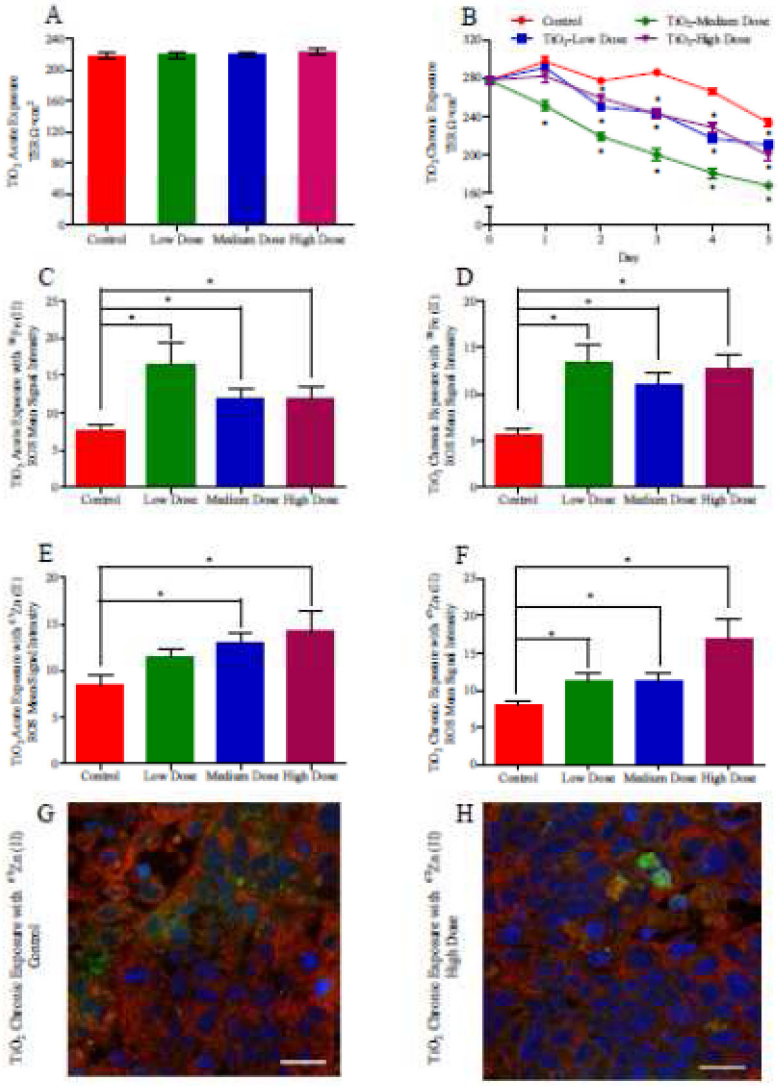

Figure 2.

Transepithelial Electrical Resistance (TER) and reactive oxygen species generation (ROS) of Caco-2/HT29-MTX monolayers following acute and chronic exposure to TiO_2 nanoparticles (NP). TER after a 4-hour exposure to low, medium, or high doses of TiO_2 NP (A). TER measurements after chronic exposure low, medium, or high doses of TiO_2 NP, medium containing NP was changed very day and TER was measured every 24 hours. * denotes significant differences according to a one-way ANOVA with Tukey's posttest ($p < 0.05$, $n = 12$) (B). ROS production in response to of acute (C and E) and chronic (D and F) doses of TiO_2 with ^{58}Fe (C and D) and ^{67}Zn (E and F). Data shown is mean±SEM, * denotes significance according to an unpaired Student's t-test, $p < 0.05$, $n = 6$. Confocal microscopy of the *in vitro* epithelium immunofluorescently stained for occludin (red), which is an integral plasma-membrane protein located at the tight junctions [91] after acute chronic exposure to an acute high TiO_2 dose with ^{67}Zn (H). The control (G) was exposed to ^{67}Zn,

but not NP. DNA (blue) is stained with DRAQ5, ROS (green) is stained with CellROX® Reagent. Scale bars are 20 μm.

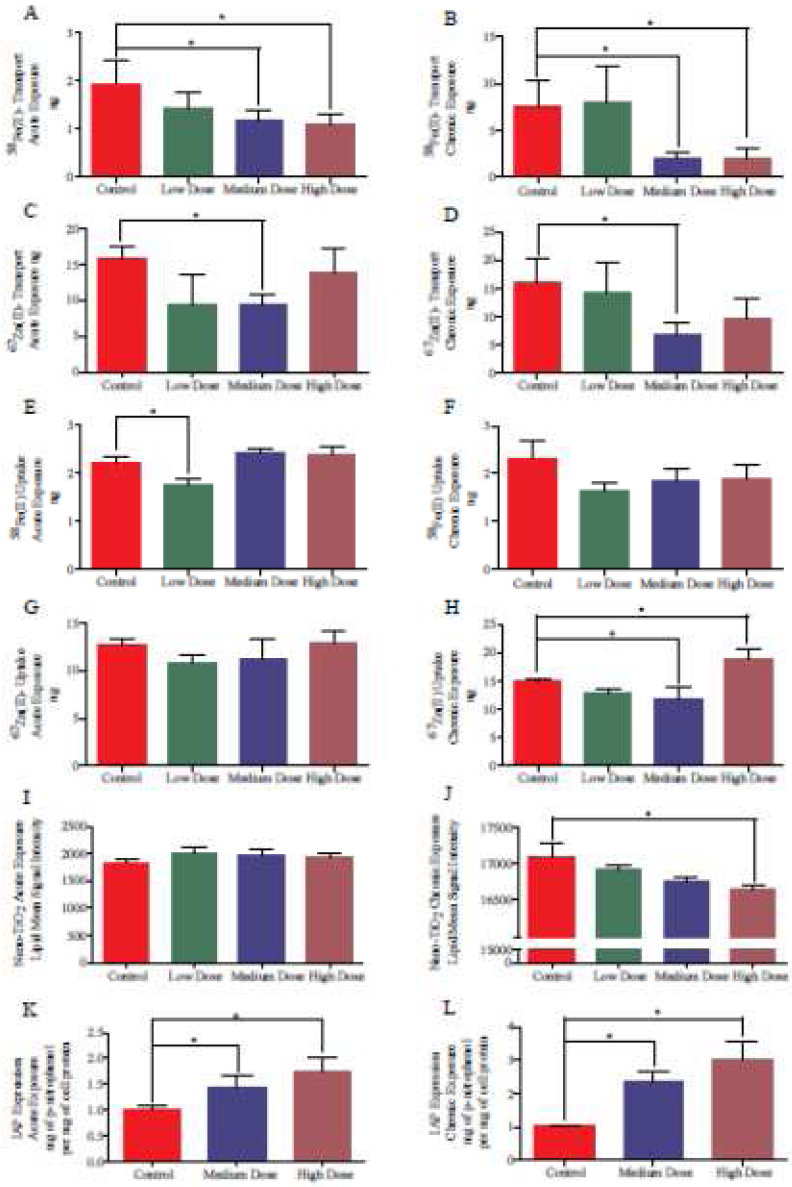

Figure 3.

Nutrient transport and brush border membrane expression. ^{58}Fe transport (A and B) or uptake (E, F), ^{67}Zn transport (C and D) or uptake (G, H), fluorescent BODIPY® 500/510 C1, C12 lipid uptake (I and J), and alkaline phosphatase activity (K and L) in response to acute (A, C, E, G, I, K) and chronic (B, D, F, H, J, L) doses of TiO_2. Data is mean±SEM. * denotes significance according to an unpaired Student's t-test, $p < 0.05$, $n \geq 6$.

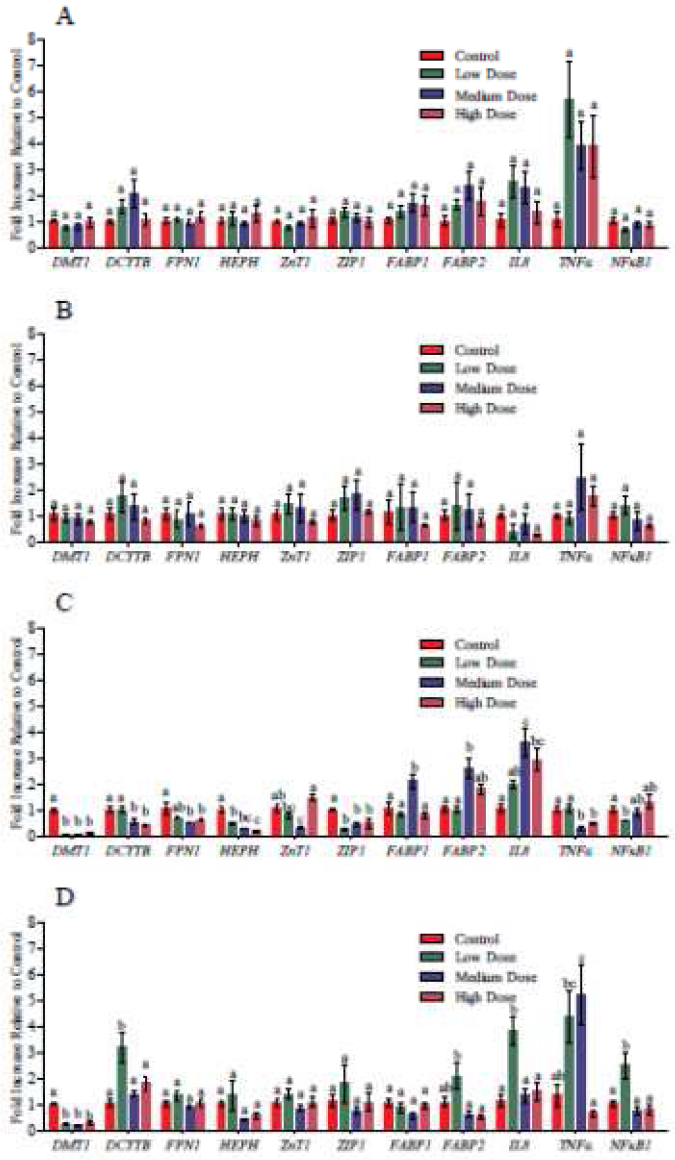

Figure 4.

Gene expression in response to of acute (A, B) and chronic (C, D) doses of TiO_2 with ^{58}Fe (A, C) and ^{67}Zn (B, D). Bars that do not share any letters are significantly different according to a one-way ANOVA with Tukey's posttest ($p < 0.05$).

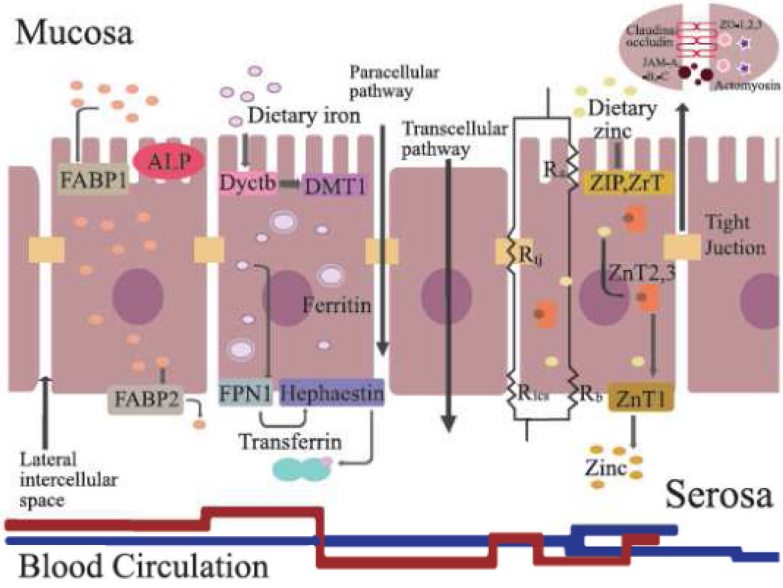

Figure 5.

Molecular nutrient transporters and brush border enzymes in the intestinal epithelium. Cell membrane proteins (DcytB, DMT1, HEPH, FPN1, ZnT1, ZIP1, SGLT-1, L-FABP, I-FABP) transporting nutrient through the intestinal epithelial cells. The transepithelial electrical resistance comes from junctions between epithelial cells and is composed of tight junction resistance (R_{tj}), intercellular space resistance (R_{ics}), apical membrane resistance (R_a); basolateral membrane resistance (R_b)[92]. Tight junctions are constructed by integral transmembrane proteins—claudins, occludin and junctional adhesion molecules (JAM-A, -B and -C) between the lateral intercellular space, and are fixed on actomyosin cytoskeleton filaments through scaffolding proteins, for example zonula occludens (ZO-1, ZO-2, and ZO-3) [93]. Intestinal alkaline phosphatase (IAP) regulates absorption of lipids across the apical intestinal epithelial membrane[88].

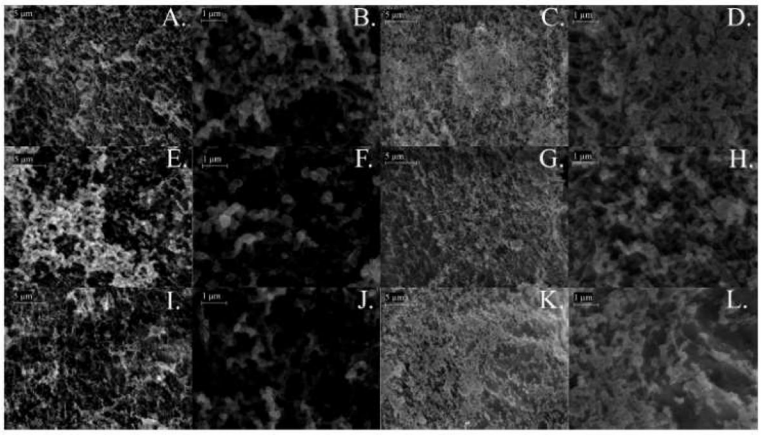

Figure 6.

Scanning electron microscopy (SEM). SEM images of control (A–D), acutely exposed to medium (E, F) or high (I, J) doses of nano-TiO_2, or chronically exposed medium (G, H) or high (K, L) doses of nano-TiO_2. The microvilli on the apical surface of *in vitro* model was exposed to TiO_2 NPs acutely (column 1 and 2) and chronically (column 3 and 4). Scalebars are 5 μm in panels A, E, I, C, G, K (magnification 10K), and 1 μm in panels B, F, J, D, H, L (magnification 40K).